

Article

Experimental Evaluation of Fire Resistance Limits for Steel Constructions with Fire-Retardant Coatings at Various Fire Conditions

Tatiana Eremina ¹, Dmitry Korolchenko ^{1,*} and Denis Minaylov ²

¹ Department of Integrated Safety in Construction, Moscow State University of Civil Engineering, Yaroslavskoye Shosse, 129337 Moscow, Russia; main@stopfire.ru

² Russian Research Institute for Fire Protection (VNIPO), Ministry of the Russian Federation for Civil Defense, Emergencies and Elimination of Consequences of Natural Disasters (EMERCOM of Russia), 143903 Balashikha, Russia; 4.3.2@vniipo.ru

* Correspondence: da-vip@mail.ru

Abstract: The experimental evaluation of fire resistance limits for steel constructions with fire-retardant coatings consists of a lot of experiments on the heating of steel structures of buildings by solving a heat engineering problem at various fire conditions. Building design implies the assessment of compliance of actual fire resistance limits for steel constructions with the required limits. Fire resistance limits for steel constructions are determined for “standard” temperature mode, and this can lead to overestimated fire resistance and underestimated heat influence for a real fire. Estimation of the convergence for “standard” temperature mode and possible “real” fire mode, as well as of the compliance of actual fire resistance limits with real fire conditions, was realized in the following stages: mathematical modeling of real fire development by the field model in software package Fire Dynamics Simulation (FDS) with various fire loads and mathematical modeling of steel construction heating for the standard temperature mode obtained by modeling “real” fire modes (the finite difference method of solving the Fourier heat conduction equation at external and internal nonlinearities was used for modeling the process of steel structure heating with the implementation in the ANSYS mechanical software package). Experiments of the assessment of fire-protective paint’s effectiveness were carried out for standard temperature mode and obtained by modeling “real” fire modes. The equivalent fire duration dependence on fire load type was determined. This dependence can be taken into account in determination of fire resistance limits for steel constructions in warehouse building roofing. Fire-protective paint effectiveness was estimated for “standard” temperature mode and various other temperature modes.

Keywords: steel structure; standard temperature mode; fire-retardant material; fire resistance estimation; fire dynamics simulator software package



Citation: Eremina, T.; Korolchenko, D.; Minaylov, D. Experimental Evaluation of Fire Resistance Limits for Steel Constructions with Fire-Retardant Coatings at Various Fire Conditions. *Sustainability* **2022**, *14*, 1962. <https://doi.org/10.3390/su14041962>

Academic Editors: Pramen P. Shrestha and Syed Minhaj Saleem Kazmi

Received: 14 November 2021

Accepted: 28 January 2022

Published: 9 February 2022

Publisher’s Note: MDPI stays neutral with regard to jurisdictional claims in published maps and institutional affiliations.



Copyright: © 2022 by the authors. Licensee MDPI, Basel, Switzerland. This article is an open access article distributed under the terms and conditions of the Creative Commons Attribution (CC BY) license (<https://creativecommons.org/licenses/by/4.0/>).

1. Introduction

Compliance with normative requirements for steel construction fire resistance limits can be confirmed by experiments or calculation methods for standard temperature mode conditions [1–4].

Standard temperature mode is a simple method for the assessment of building construction fire resistance limits, which does not take into account the peculiarities of fire development and spread in buildings. Frequently, the design of big logistic centers (warehouses) with their technological processes demonstrate the essential difference between fire development dynamics (and “real” temperature modes) and “standard” temperature mode. Therefore, the method of computer modeling of fire development can be used for such buildings because of the high cost and impossibility of actual large-scale fire tests. Software packages such as the Fire Dynamics Simulator (FDS), Phoenix, Fluent, Sofie,

and the home-grown technology of professor Puzach S. are widespread nowadays and present differential equation solutions (field method), taking into account that many factors influence the dynamics of the dangerous factors of fire (space-planning solution, ventilation, automatic fire suppression system, smoke-control system, wind, fire extinguishing agents by fire brigades, etc.).

Warehouse building design assumes fire resistance level compliance with the fire safety requirements taking into account approved design solutions. The evaluation of this compliance is fulfilled for the standard temperature mode, and the application of this mode can lead to overestimated fire safety parameters and the underestimation of heat influence.

The purpose of the research is to evaluate correct application of standard fire test results for a modern warehouse building design with fire protection and without it.

The following tasks were solved to achieve this purpose:

1. The modeling of fire spread in a warehouse building for various fire loads accepted in the Russian Federation on the basis of multi-year experimental research taking into account international experience;
2. Modeling of load-bearing construction heating for standard temperature mode and for temperature modes from modeling process;
3. The equivalent fire duration was determined for load-bearing constructions and the experimental evaluation of burning characteristics for fire-retardant paints were fulfilled for various heat flows.

The practical value of the work is in reducing the number of experiments on evaluation of fire resistance limits for steel constructions with fire-retardant coatings at various fire conditions. The novelty of the investigation is the consideration of real fire load. The hypothesis is that the behavior varies for structures with fire protection and without it.

The structure fire resistance rating is the time interval from the beginning of fire exposure under standard testing conditions until one.

The structure with the actual fire resistance rating retains its load-bearing function for the period of time necessary to ensure safety:

$$R_f > R_{req} \quad (1)$$

where R_f is the actual fire resistance rating value of the structure and R_{req} is the required fire resistance rating value of the structure.

Many scientists investigated the evaluation of fire resistance for steel constructions including J. Kruppa [5], I. Dorn [6], D. Tohr [7], A. Yakovlev [8], I. Molchadsky [9], V. Roitman [10], and V. Golovanov [11].

This work is about the evaluation of the influence of real temperature mode on fire-protective properties of fire-retardant paints and the fire resistance of steel constructions.

In order to estimate the equivalent fire duration, heat engineering calculations were carried out for the steel structures of a building when it was exposed to the temperature conditions of a standard curve and at exposure to the fire temperature conditions. Standard temperature conditions, as well as fire temperature conditions, were considered for the evaluation of the fire resistance of steel structures of the building. The field mathematical model in Fire Dynamics Simulator (FDS) software package was used for the modeling of fire temperature conditions.

In this work, the software complex FDS was used for the modeling of fire modes in enclosures. The heat calculation for steel constructions was fulfilled in the software complex ANSYS, using finite element methods for heat conductivity tasks.

Nowadays, many software complexes provide 3D fire modeling, as well as heating processes for steel constructions (some of them are presented at [International Survey of Computer Models for Fire and Smoke. Available online: www.firemodelsurvey.com (accessed on 13 November 2021)].

The most widespread software for field mathematical modeling (solving differential equations) of a fire in the United States and in our country is the Fire Dynamics Simulator

6 (FDS) (NIST, Gaithersburg, MD, USA) software package, which has certain verification and validation features to determine the real temperature modes of fires. The FDS was developed by the National Institute Standards and Technologies (NIST).

Systems of non-stationary equations for fundamental physical laws (conservation of mass, impulse, and energy) can be solved in FDS by modern numerical algorithms.

Numerical methods for Navier–Stokes differential equations (field method of fire spread modeling) provide proper modeling of fire for every stage of its development [12].

Temperatures are actualized in time by the Crank-Nicolson implicit scheme based on numerical approximation for the solutions in an intermediate point $(x, t + \tau/2)$. The discrete method of radiant heat transfer calculation was applied for radiance flow modeling.

This method is based on the calculation of radiation in the selected characteristic directions in the room between the walls (or surfaces limiting the calculation area) with the subsequent calculation of heat loss by radiation in the energy equation for each control volume. Two types of combustion models are used in the FDS software package: the combustion model for direct numerical simulation (DNS) and the combustion model for large eddy simulation (LES). The radiative heat transfer model solves the radiative heat transfer equation in a non-scattering gray atmosphere. In the fire model in the FDS software package, the system of equations is approximated on one or more linear grids. Combustible materials and building structures are represented by rectangular objects that correspond to the main grid. Thermophysical characteristics are assigned to all surfaces of combustible materials and building structures. The basic principle for determining the temperature in a room during a fire is associated with the law of conservation of energy. The conservation of energy for each zone considered is expressed in the fact that the energy added to the zone is equal to the energy lost by the zone. The energy produced by the fire and added to this zone is equal to the energy lost by the zone through radiation and convection, plus the energy lost by the zone through the openings of the room.

The stability of materials and structures in operation and under fire exposure conditions is associated with the creation of new effective types of flame-retardant coatings. The halogen-free, flame-retardant, waterborne polyurethane, and eco-friendly coatings have synergistic effects [13–20]. Using recombinant adhesive proteins as durable and green flame-retardant coatings was considered.

The thermal effect on the flame-retardant coating, regardless of whether the effect comes from the substrate or from the outside, can cause reversible and irreversible processes.

The former is associated with the weakening of intermolecular interaction in the structure of the coating and characterize heat resistance, and the latter is associated with the breakage of chemical bonds: these processes reflect thermal resistance. Irreversible chemical changes in the structure of the flame-retardant coating are associated with their chemical bond energy. The paint composition components—pigments, plasticizers, and other additives—significantly affect heat aging [21–23]. The degradation of coatings slows down in the presence of pigments with reflective properties or acting as heat stabilizers, and, on the contrary, it accelerates when pigments serve as catalysts or initiators of chemical processes.

Figures 1 and 2 show examples of flame-retardant coatings for steel structures.

Most buildings consist of metal structures (Figures 1 and 2). The development of a methodology for assessing the flammability of building materials and structures is necessary to reduce the flammability of materials with flame-retardant coatings [22,23]. It should be noted that in the process of operation, the building materials and structures are subjected to structural change processes. One such process is heat aging, which is also a prime example of the impact of anthropogenic factors, in particular operation in elevated temperature conditions.



Figure 1. Steel beam fire protection.



Figure 2. Vertical steel member fire protection.

2. Materials and Methods

Steel metal structures are the main supporting framework of buildings, and their strength and fire resistance play a key role in fire conditions. Various methods and means of protection are used to increase the fire resistance limits of structures. It is known that one of the effective ways to protect steel structures in case of fire is thin-layer polymer coatings that can increase many times when heated. The fire-retardant coatings are multi-component formulas. The basis of a fire-retardant coating is a polymeric binder and fillers, as well as stabilizers of the foamed coal layer. In case of fire, the coating structure bloats, and a fine-meshed layer of coating with low thermal conductivity is formed, as a result of which the heating of metal structures is slowed down dramatically and the limit state is achieved before the loss of strength at 500 °C.

2.1. Warehouse Description

Steel structures were used as the building's load-bearing elements. Farms are made of bent-welded profiles, and horizontal links are made of bent-welded profiles. The building has two gates and the entrance door. The walls of the building contain 32 windows. The following were accepted as the fire load in accordance with reference data [13,14]: textile products, rubber and its products, ethyl alcohol, cables and wires, shredded cotton, paper in rolls, packaging (wood, cardboard, and polystyrene), radio materials, industrial oil, and cotton in bales. Identifying the attributes of a profession in the practice and regulation of fire safety engineering were investigated by [15]. The application of the integration of BIM, IoT, and AR/VR technologies for fire safety was analyzed in recent studies [16–18].

The paint chosen for this study is proposed to be tested by standard temperature mode according to the GOST 30247.0 and by various heat flows.

Fire tests of the paint for the standard temperature mode were carried out at a steel column according to the GOST R 53295-2009. The test specimen was the I-shaped steel column №20 according to the GOST 8239-89 with a height of 1.7 m (metal effective thickness of 3.4 mm). The undercoat layer thickness GF-021 was 0.05 mm. The paint thickness A was 0.85 mm.

The radiative panel according to the GOST 30402 was used to estimate heat flow influence on paint characteristics. The test specimens were carbon steel metal plates of 100×100 mm, with a thickness of 3 mm. The steel plate temperature was recorded by two thermocouples TXA (K) located on an unheated surface. The thermocouples were located in the center related to the specimens with a distance of 30 mm between them. The undercoat thickness GF-021 was 0.05 mm. The paint thickness A was 0.5 mm.

The evaluation of the fire resistance rating of the building structures with flame-retardant coatings according to the standard fire test temperature conditions, without taking into account the specific fire load or the control of fire protection coatings, can lead to an underestimation of the actual fire resistance rating, which negatively affects the safety of the entire building [24–28]. This is particularly relevant when examining structures under the effect of anthropogenic factors (fire), including emergency situations. For example, this is relevant for metal structures (Table 1).

Table 1. Analysis of flame-retardant coatings for metal structures.

Description	Fire Resistance Rating—Mass Factor	Dry Layer Thickness, mm—Flow Rate, kg/m ²	Drying Time, h	Indoor/Outdoor Application	Type (Base)
Unikum flame-retardant paint for steel structures	R45-2.4 R60-3.4	0.8–0.6 1.2–0.9	12	indoors	water
BICOAT FIRE 101 brand flame-retardant paint for steel structures	R45-3.4 R60-3.4	0.85–1.51 1.25–2.23	4	indoors	organic
DEKOTERM R flame-retardant paint for steel structures	R45-3.4 R90-5.8	0.87–1.48 1.75–2.95	6	indoors	organic
OZK-45 brand flame-retardant paint for steel structures	R45-3.4 R60-3.4 R90-5.8	1.07–1.93 1.72–3.10 1.77–3.19	8	indoors	water
EKOTERM-S brand flame-retardant paint for treatment of steel structures	R90-5.8	1.71–2.52	6	indoors	water

Steel used for the manufacture of load-bearing building structures, being a non-combustible material, changes its properties when exposed to high temperatures. Fire resistance ratings for most unprotected metal structures are in the R10 range. The reasons for such low fire resistance ratings are the high thermal conductivity of metal and a decrease in strength characteristics when exposed to heat, as well as the development of thermal and plastic deformations.

Data for steel: density of 7800 kg/m³, heat conductivity coefficient of $48-3.65 \cdot 10^{-2} T$ Wt/m °C, specific heat capacity of $0.44 + 4.8 \cdot 10^{-4} T$ kJ/kg °C, and emissivity factor of 0.74.

The results of the steel thermal characteristics changing were obtained experimentally and presented in [29–33].

2.2. Research Methods

The evaluation of the correct application of some standard fire test results for a modern warehouse building was investigated in this study.

The following objectives were formulated: the choice of real fire load and the choice of equivalent fire duration.

The method allows us to reduce the number of experiments on the evaluation of fire resistance limits for steel constructions with fire-retardant coatings at various fire conditions.

The results can be achieved by FDS simulation. The research is presented according to the standard temperature mode for various fire loads: cables and wires, industrial oil, and ethanol.

The methods, used to study the operational properties under the effect of anthropogenic factors (fire), consider the factors that may affect the reduction of fire protection efficiency of the coating. For example, a large number of hydrophobic flame-retardant coatings lose from 50% to 100% of their fire protection efficiency after a month in actual operating conditions due to the accumulation of moisture and various aggressive vapors and gases. The limit state is the state of the structure in which it ceases to meet the operational requirements, i.e., it either loses the ability to resist external impacts or receives unacceptable deformation or local damage, causing further operation to be unacceptable or inexpedient.

The actual fire resistance rating is determined using GOST 30247.1-94 or using calculation methods.

In GOST 30247.1-94 (Building Structures. Fire Resistance Test Methods. Load-Bearing and Enclosing Structures), the limit state for the load-bearing capacity loss is the structural collapse or ultimate deformations (R). In addition, this document regulates the limit states for thermal insulating capacity (I), which is limited by reaching the limit temperatures on the unheated surface, as well as loss of integrity (E) when holes and cracks occur, leading to the combustion products and flames entering through them. The assessment of fire protection efficiency of flame-retardant coatings for metal structures is carried out using GOST R 53295-2009, "Fire Retardants for Steel Structures. General Requirements. Method for Determining Fire Protection Efficiency", which describes the method for determining the time of reaching the limit state, characterized by the critical temperature inside the sample or on its unheated side.

The ventilation opening in this study was the object simulating the fire load in FDS software package. In order to assess the temperature on the surface of steel structures of the upper truss belt, sensors (thermocouples) were placed with a pitch of 1 m, and the average volume temperature at the height of 4.7–6.5 m was also measured. During the calculations, the gates of the building were open, while the windows were closed.

The load-bearing structures of the building cover are shown in Figure 3.

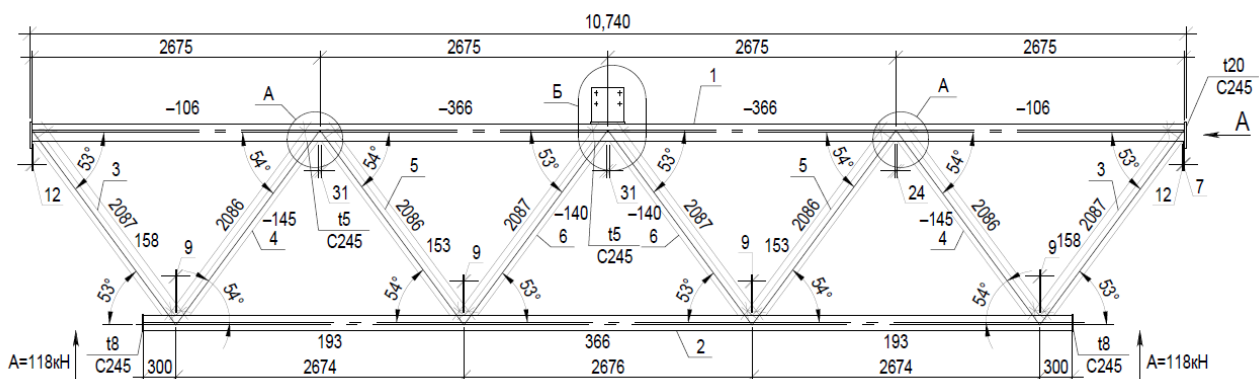


Figure 3. Structural elements with various cross-sections and thicknesses (dimensions in mm).

The structural element dimensions are shown on the Table 2.

Table 2. Structural element dimensions.

Element	Cross-Section	Dimensions, mm	Cross-Section Area, mm ²	Perimeter of Heated Surface, mm	Effective Metal Thickness, mm
1	rectangular	a = 160, b = 160, h = 5	3100	640	4.84
2	rectangular	a = 140, b = 140, h = 5	2700	560	4.82
3	rectangular	a = 100, b = 100, h = 5	1900	400	4.75

The calculation was performed under the condition of temperature change of the heating medium in the time along the standard fire curve (Table 3).

Table 3. Calculation parameters.

Parameter	Formula	Note
Coefficient α , W/(m ² deg), from the heating medium with temperature t_B , τ to the surface with temperature t_0	$\alpha = \alpha_c + \alpha_r + 29 + 5.77xS_r x \frac{\left(\frac{T_B}{100}\right)^4 - \left(\frac{T_0}{100}\right)^4}{T_B - T_0}$	α_c —the convective factor; α_r —the radiant factor; s_r —the reduced emissivity factor of the heating medium and structure surface.
Reduced emissivity factor	$S_r = \frac{1}{\frac{1}{s} + \frac{1}{s_0} - 1}$	s —the emissivity factor of the furnace fire chamber. $S = 0.85$; s_0 —the emissivity factor of the heated surface of the structure; $s_0 = 0.74$ for unprotected steel structures.

The calculation of the temperature of the structure metal rod was performed according to the algorithm, which represents a number of formulae obtained on the basis of solving the boundary problem of heat conductivity of elementary balance methods (finite difference method of solving the Fourier heat conduction equation at external and internal non-linearities).

The temperature of steel structures was calculated using the above formulae sequentially in the calculated time intervals $\Delta\tau$ up to a given critical value. The initial temperature at all points of the structure cross-section before the fire and ambient temperature outside the fire zone was determined to be 20 °C ($t_h = 293$ °K). The value of the calculated time interval $\Delta\tau$ (program pitch) was selected so that it would fit an integer number of times in the interval of the machine record of the calculation results; the selected value $\Delta\tau$ would not exceed the value calculated using the formula in Table 4.

Table 4. Calculation parameters of steel structures.

Parameter	Formula	Note
Maximum design time interval $\Delta\tau_{max}$	$\Delta\tau_{max} = \frac{\gamma_{sw} \cdot \delta_{ef} \cdot (C + D_{cm} \cdot t_{cm})}{\alpha}$	γ_{sw} — metal specific weight, kg/m ³ ; α and t_{cm} — maximum possible values in the calculation; C — metal heat capacity coefficient, J/(kg deg); D_{cm} — coefficient of metal heat capacity change at heating, J/(kg deg ²); δ_{ef} — effective thickness of metal, m; $\delta_{ef} = \frac{F}{P}$, F —cross-sectional area of the rod, m ² ; P —heated perimeter of the rod cross-section, m.
Algorithm for calculating the temperature of unprotected metal structures	$t_{cm, \Delta\tau} = \frac{\Delta\tau}{\gamma_{sw} \cdot \delta_{ef} \cdot (C + D_{cm} \cdot t_{cm})} \cdot \alpha \cdot (t_{B, \tau} - t_0) + t_h$	$t_{cm, \Delta\tau}$ —rod temperature in the calculated time interval $\Delta\tau$, °K; t_{cm} —rod temperature at a given time τ , °K; $t_{B, \tau}$ —temperature of the heating medium at a given time τ , °K; α —heat transfer coefficient from the heating medium to the structure surface, W/(m ² deg); C_{cm} —initial metal heat capacity coefficient, J/(kg deg); D_{cm} —coefficient of change of heat capacity of metal at heating, J/(kg deg ²); γ —metal specific weight, J/(kg/m ³); δ_{ef} —effective thickness of metal, m.

Models of farm elements were constructed for the thermal engineering calculation in the ANSYS mechanical software package.

The analytical model was used to estimate the heat transfer and flame retardancy under different heat fluxes. While the heat transfer model adopted for the experimental gas furnace and electric furnace installations is widely known [34–40], it is also applicable to steel specimens protected by intumescent coatings and has been tested in a “mass loss cone calorimeter” installation.

The heat transfer mechanism between the heater and the protected steel plate is shown in Figure 4.

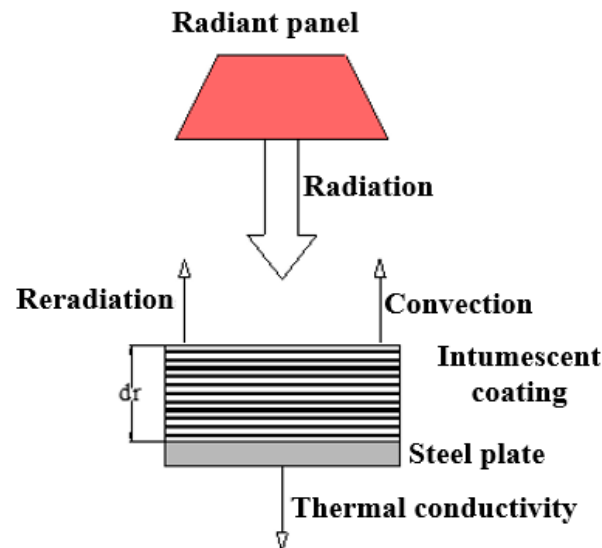


Figure 4. Schematic heat transfer model for an intumescent flame-retardant protected steel plate.

As with unprotected steel, the specimens are exposed to the heat flux at the surface level. In contrast to the heat transfer model for an unprotected steel plate, the presence of an insulating material (intumescent coating) reduces the temperature penetration rate through the steel plate. Moreover, in the study [34–39], the heat transfer model includes three types of different heat losses between the heat source and the steel sample. When the steel is heated, it transfers heat to the environment in the form of convection (convective heat transfer coefficient αc) and reradiation (steel radiation coefficient ϵs). In addition, a small amount of heat energy is dissipated from the bottom of the steel plate sample through the insulating material.

The mathematical model is based on the assumption that the heat flux is one-dimensional and that the radiant plate and the steel sample with the flame-retardant coating are treated as two parallel planes. In this model, the radiative and absorptive capacities of the intumescent coating are assumed to be constant. The authors of [19,20] confirmed that good results were obtained considering a constant emissivity of 0.92, which is close to the values obtained in other studies [40–42]. In addition, the mathematical model assumes that the intumescent coating has a density of 1000 kg/m^3 and a specific heat capacity of $1000 \text{ J/kg}\cdot\text{K}$. As the heat absorbed by the intumescent coating is extremely low, there is no need to apply exact values of the intumescent coating temperature, density, and specific heat capacity.

The heat transfer model described is derived from simple thermal balance equations: at the boundaries of the steel sample, the amount of heat passing through the conical heater to the steel sample is equal to the amount of heat released by the steel sample through convection and radiation and to the amount of heat absorbed by the intumescent paint and steel to increase their temperature (heat energy increment).

Based on this, the heat quantity Q (J) passing through the radiant panel to the insulated steel section during the time interval t can be expressed as:

$$\Delta Q = \alpha_p q_r A_s \Delta t - Q_{loss} \Delta t, \quad (2)$$

where α_p is the absorption capacity of the intumescent paint, q_r is the heat flux from the cone heater to the protected plate surface (W/m^2), A_s is the area of the exposed steel surface (m^2), Δt is the time increment (s), and Q_{loss} is the heat loss from the opposite side of the plate (J/s).

On the other hand, the amount of thermal energy ΔU (J) emitted and absorbed by the protected steel sample can be expressed as:

$$\Delta U = \left[\varepsilon_p \sigma T_p^4 + h_c (T_p - T_a) \right] \cdot A_s \Delta t + \frac{\Delta T_p + \Delta T_s}{2} \rho_p c_p A_p d_p + \Delta T_s \rho_s c_s A_s d_s \quad (3)$$

where ε_p is the radiating capacity of the intumescent paint, and $\varepsilon_p = 0.92$; σ is the Stefan–Boltzmann constant ($5.67 \cdot 10^{-8} \text{ W}/\text{m}^2 \cdot \text{K}^4$); T_p is the surface temperature of the intumescent paint (K); h_c is the convective heat transfer coefficient ($20 \text{ W}/\text{m}^2 \cdot \text{K}$); T_a is the ambient temperature (K); A_s is the area of the open steel surface (m^2); Δt is the time increment (s); ΔT_s is the steel temperature increment ($^\circ\text{C}$); ΔT_p is the intumescent paint surface temperature increment (K); ρ_p is the intumescent paint density ($1000 \text{ kg}/\text{m}^3$); c_p is the specific heat capacity of the intumescent paint ($1000 \text{ J}/\text{kg} \cdot \text{K}$); A_p is the area of intumescent paint surface (m^2); d_p is the thickness of the intumescent paint dry film (M); ρ_s is the steel density (kg/m^3), and $\rho_s = 7850 \text{ kg}/\text{m}^3$; c_s is the specific heat capacity of steel ($\text{J}/\text{kg} \cdot \text{K}$); and d_s is the plate thickness (m).

Considering the above formulae, the heat transfer model for protected steel specimens can be obtained by comparing Formulas (3) and (4), i.e., the boundary of the steel specimen the amount of heat ΔQ passing through the radiant panel to the steel section during the time interval Δt is equal to the amount of heat energy ΔU emitted and absorbed by the steel substrate:

$$\alpha_p q_r - \frac{Q_{loss}}{A_s} = \varepsilon_p \sigma T_p^4 + h_c (T_p - T_a) + \frac{\Delta T_p + \Delta T_s}{2 \Delta t} \rho_p c_p d_p + \frac{\Delta T_s}{\Delta t} \rho_s c_s d_s \quad (4)$$

Equation (4) has three uncertain variables: the absorption capacity of the intumescent paint α_p , the heat loss from the opposite side of the plate Q_{loss} through the thermal insulation material, and the surface temperature of the intumescent paint T_p . The heat accumulated in the intumescent coating is very low when the intumescent paint has reached its full expansion. In addition, the heat accumulated in the steel plate is a relatively small amount. Thus, we can state that after reaching the quasi-stationary conditions of the system, the surface temperature of the intumescent coating should approach a constant value, which depends on the radiation level. Consequently, the heat flux value generated by the radiant panel is much larger than that of the other three variables of the formula, and thus they can be neglected.

However, the temperature of the intumescent coating T_p is very difficult to estimate, and it can only be estimated using sophisticated equipment, such as the thermographic phosphor method. Thus, without this information it is not possible to determine the thermal conductivity of the intumescent coating for this experimental setup.

Following the previous approach, the thermal conductivity of the intumescent coating can be obtained using the following formula:

$$\lambda_p \left(\frac{T_p - T_s}{d_p} \right) - Q_{loss} = \frac{\Delta T_p}{\Delta t} \rho_s c_s d_s \quad (5)$$

As Q_{loss} is negligible, T_p can then be calculated using Formula (6), which can ultimately be expressed as follows:

$$\varepsilon_p \sigma T_p^4 + h_c (T_p - T_a) = q_r, \quad (6)$$

Thus, by recording ε_p , σ , h_c , T_a , and q_r , we can calculate the temperature surface T_p of the intumescent coating and p. The thermal conductivity (equivalent) is obtained using Formula (5), applying the initial thickness of the dry coating layer. As the surface temperature of the intumescent coating is difficult to estimate and can only be done using

special equipment (thermographic phosphor method), in this work, the paint surface temperature was calculated using Formula (6). The data used for calculation were as follows:

- heat flux 20 kW/m², 30 kW/m², 40 kW/m², and 50 kW/m²;
- $\varepsilon_p = 0.95$;
- T_a is the temperature is measured inside the plate;
- σ is the Stefan–Boltzmann constant.

The obtained calculation results are as follows: for 20 kW/m²— $T_p = 355$ °C, for 30 kW/m²— $T_p = 470$ °C, for 40 kW/m²— $T_p = 554$ °C, and for 50 kW/m²— $T_p = 620$ °C.

The following approach was also suggested to evaluate the efficiency of the intumescent coating. Specifically, the ability of the intumescent coatings to reduce heat penetration and the temperature of the steel substrate was evaluated for efficiency considerations. The effectiveness of intumescent coatings was related to the ability of the passive fire protection system to reduce the temperature of the protected steel plate relative to the unprotected steel plate. Many different formulations were proposed, but the one with the greatest physical significance was selected. Regarding the radiant panel experiment, the temperature of the protected and unprotected steel plate increased during the test time due to exposure to radiation. After a certain amount of time, which depended mainly on the heat flux, the two temperatures reached a constant value until the end of the experiment. This aspect is related to the fact that the intumescent paint develops its coked cellular material structure in such a short period of time, but it is difficult to detect degradation. Thus, the best efficiency of the intumescent coating should be represented by an increasing function that reaches a constant value during the experiment: firstly, the paint expands and, thus, its thermal resistance increases; secondly, it retains its own thermal insulation properties.

As a result, the authors propose to express the effectiveness of the intumescent coating via the efficiency coefficient K_{ef} , which is calculated using Formula (7):

$$K_{ef} = \frac{T_{s.n.} - T_{s.p.}}{T_{s.n.}} \quad (7)$$

where: $T_{s.n.}$ is the temperature of the steel plate without intumescent coating (K) and $T_{s.p.}$ is the temperature of the steel plate with applied intumescent coating (K).

This evaluation method can be applied to analyze both the results obtained in the fired heater and under the exposure to the radiant panel. Thus, a broader understanding regarding the characteristics of intumescent coatings exposed to different fire temperature conditions can be obtained.

Moreover, in order to compare the flame-retardant properties of paint formed under fire conditions and “standard” temperature conditions, the authors propose to introduce a new concept of “fire durability of flame-retardant paint”, which characterizes the ability of paint to retain its flame-retardant properties under fire conditions. Fire durability of the examined flame-retardant paints can be estimated using efficiency coefficients calculated using Formula (8):

$$K_{fire\ durability} = \frac{K_{ef.f}}{K_{ef.i}} \quad (8)$$

where $K_{ef.f}$ is the coating efficiency under the “actual” fire conditions and $K_{ef.i}$ is the coating efficiency under the “standard” fire conditions.

3. Results and Discussion

3.1. FDS Modeling Results

The results of numerical simulation of the fire temperature conditions based on reference data are presented in Figure 5.

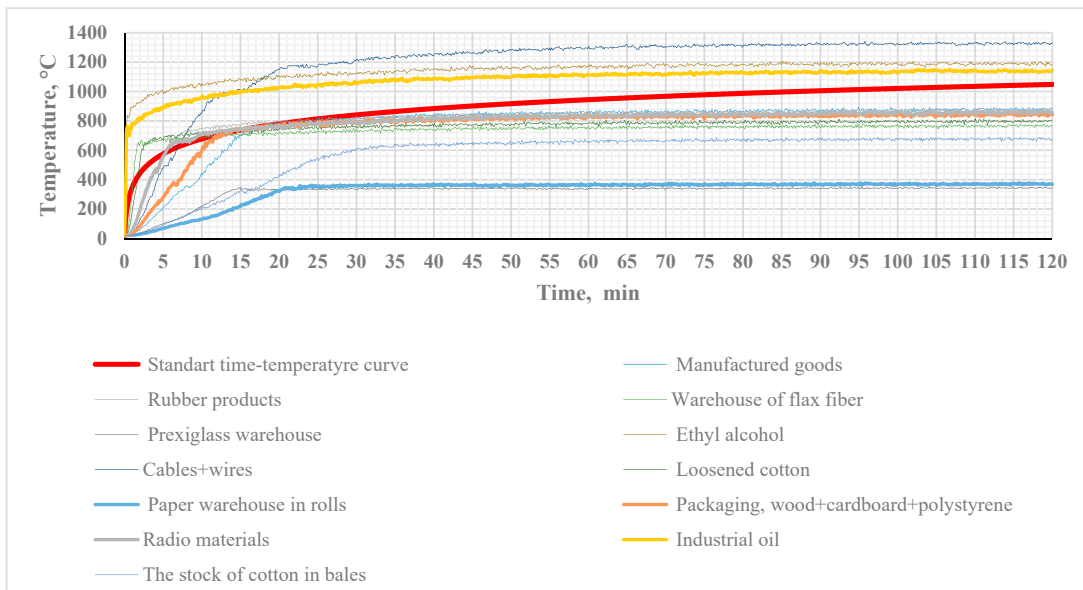


Figure 5. Modeling of standard fire temperature conditions.

The determined temperature conditions for cables and wires, industrial oil, and ethyl alcohol fire loads showed that the standard temperature conditions have lower maximum temperature values. For the rest of the fire loads specified above, the values of maximum temperatures obtained through numerical experiment are lower than under standard temperature conditions.

Heat flux values applied to the coating structures were also obtained based on the results of modeling in the FDS software package (Figure 6).

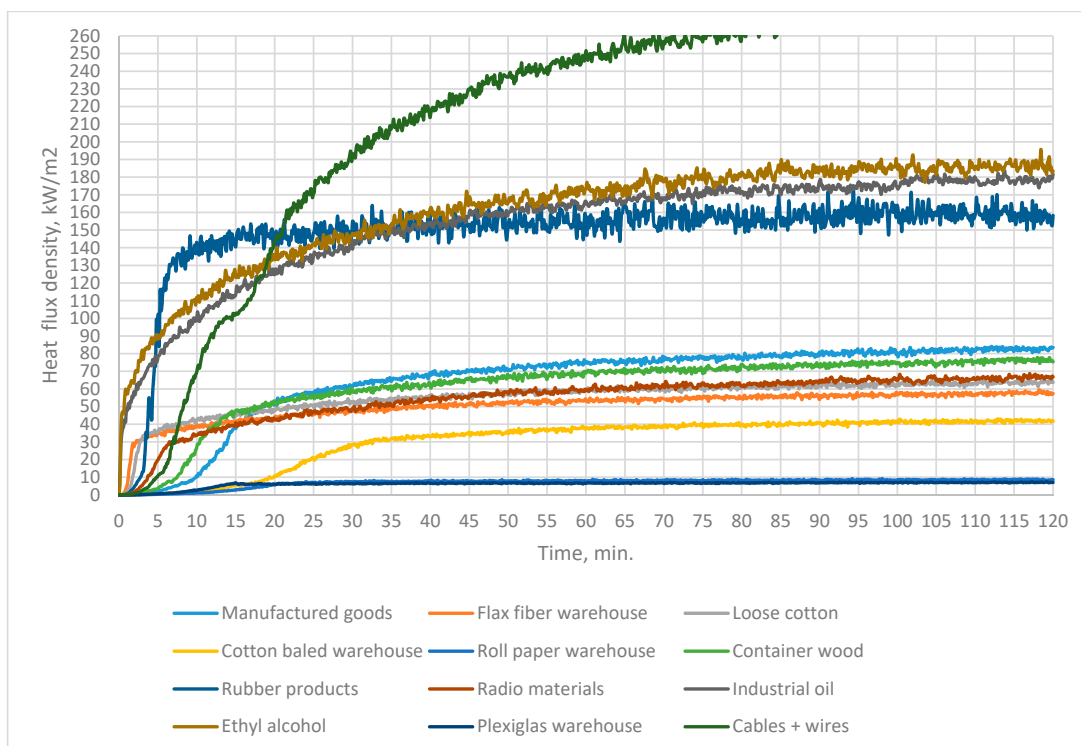


Figure 6. Heat flux values applied to coating structures.

3.2. ANSYS Modeling Results

The results of the calculations are given in Table 5 and in Figures 7–9.

Table 5. Comparative results of steel structure measurements.

Structure Type	Temperature, °C	Structure Heating Time, min.												
		1 *	2 *	3 *	4 *	5 *	6 *	7 *	8 *	9 *	10 *	11 *	12 *	13 *
160 × 160 × 5	400	6.6	13.6	7.2	4.6	-	1.7	8.2	5.0	-	11.1	7.4	2.3	24.1
140 × 140 × 5		6.6	13.6	7.2	4.6	-	1.7	8.2	5.0	-	11.1	7.4	2.3	24.1
100 × 100 × 5		6.5	13.5	7.1	4.5	-	1.7	8.1	4.9	-	11.0	7.3	2.2	24.0
160 × 160 × 5	450	7.4	14.3	7.7	5.2	-	1.9	8.6	5.6	-	11.7	8.1	2.6	25.8
140 × 140 × 5		7.4	14.3	7.7	5.2	-	1.9	8.6	5.6	-	11.7	8.1	2.6	25.8
100 × 100 × 5		7.4	14.3	7.7	5.2	-	1.9	8.6	5.5	-	11.7	8.0	2.5	25.7
160 × 160 × 5	500	8.4	15.0	8.2	6.0	-	2.2	9.0	6.2	-	12.4	8.9	2.9	27.9
140 × 140 × 5		8.4	15.0	8.2	6.0	-	2.1	9.0	6.2	-	12.4	8.9	2.9	27.8
100 × 100 × 5		8.3	15.0	8.2	6.0	-	2.1	9.0	6.2	-	12.4	8.8	2.9	27.7
160 × 160 × 5	550	9.5	15.8	8.9	7.0	-	2.4	9.5	7.1	-	13.2	9.8	3.3	30.3
140 × 140 × 5		9.5	15.8	8.9	7.0	-	2.4	9.5	7.1	-	13.2	9.8	3.2	30.3
100 × 100 × 5		9.5	15.7	8.9	6.9	-	2.4	9.4	7.0	-	13.1	9.7	3.2	30.2
160 × 160 × 5	600	10.9	16.7	9.7	8.4	-	2.7	9.9	8.1	-	14.1	10.8	3.7	34.0
140 × 140 × 5		10.9	16.7	9.7	8.3	-	2.7	9.9	8.1	-	14.1	10.8	3.6	34.0
100 × 100 × 5		10.8	16.7	9.7	8.2	-	2.6	9.9	8.1	-	14.0	10.7	3.6	33.9
160 × 160 × 5	650	12.7	17.7	10.7	10.7	-	3.0	10.3	9.7	-	15.2	12.2	4.1	52.0
140 × 140 × 5		12.7	17.7	10.7	10.6	-	3.0	10.3	9.7	-	15.2	12.2	4.1	52.0
100 × 100 × 5		12.6	17.7	10.7	10.5	-	2.9	10.3	9.6	-	15.1	12.1	4.0	52.0
160 × 160 × 5	700	15.2	19.0	12.3	16.7	-	3.3	10.8	12.6	-	17.0	14.4	4.6	-
140 × 140 × 5		15.2	19.0	12.2	16.7	-	3.3	10.8	12.6	-	17.0	14.3	4.6	-
100 × 100 × 5		15.1	19.0	12.2	16.7	-	3.2	10.8	12.5	-	16.9	14.3	4.5	-

Note. * Items in the table: 1—Standard temperature conditions; 2—industrial Goods; 3—Rubber products; 4—flax fiber Warehouse; 5—plexiglass Warehouse; 6—Ethyl alcohol; 7—Cables + wires; 8—loosened Cotton; 9—paper Warehouse in rolls; 10—packaging (wood + cardboard); 11—radio materials; 12—Industrial oil; 13—cotton Warehouse in bales. The “-” sign in the table means that the specified temperature in the table does not occur during the calculation.

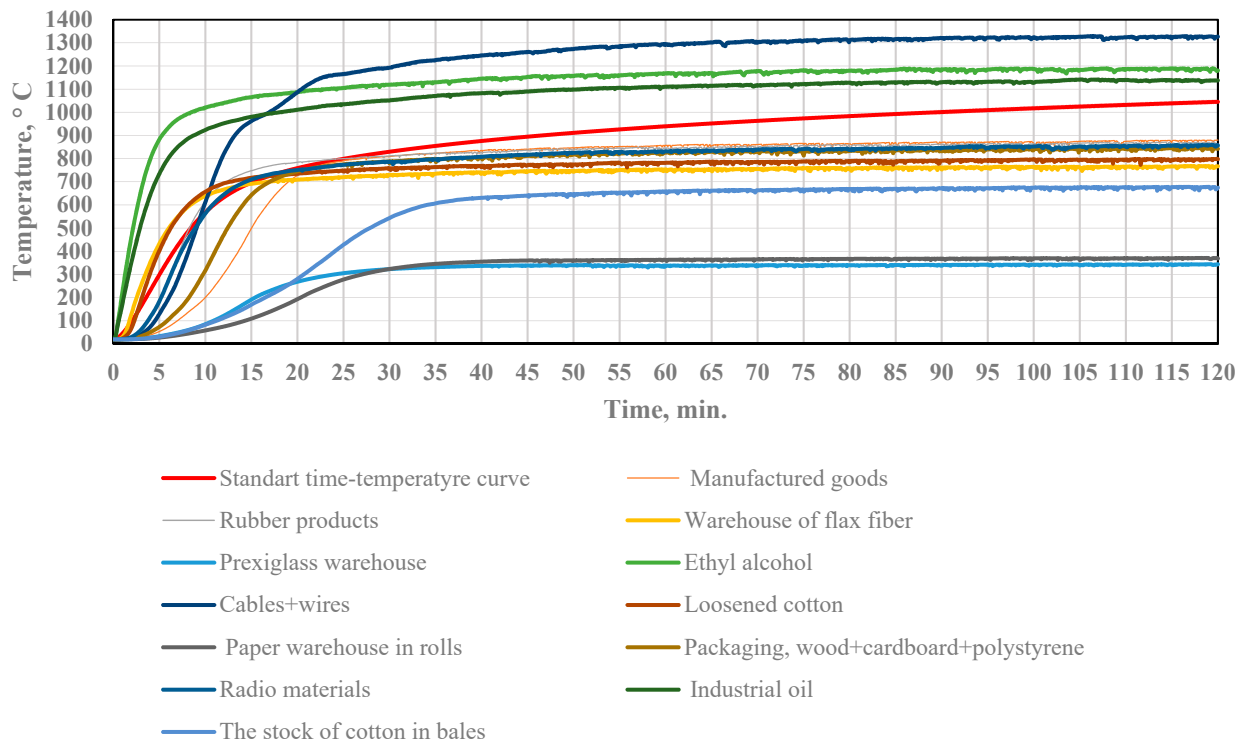


Figure 7. Rectangular 160 × 160 × 5 mm pipe.

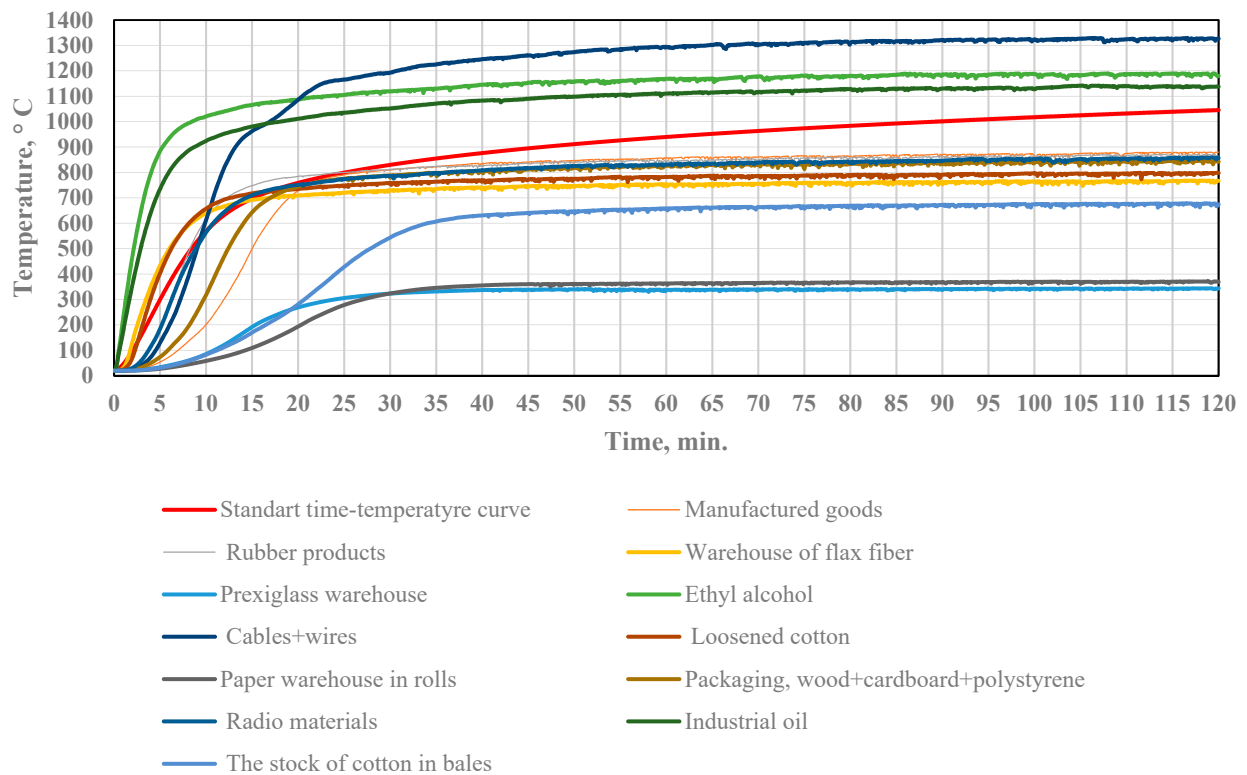


Figure 8. Rectangular 140 × 140 × 5 mm pipe.

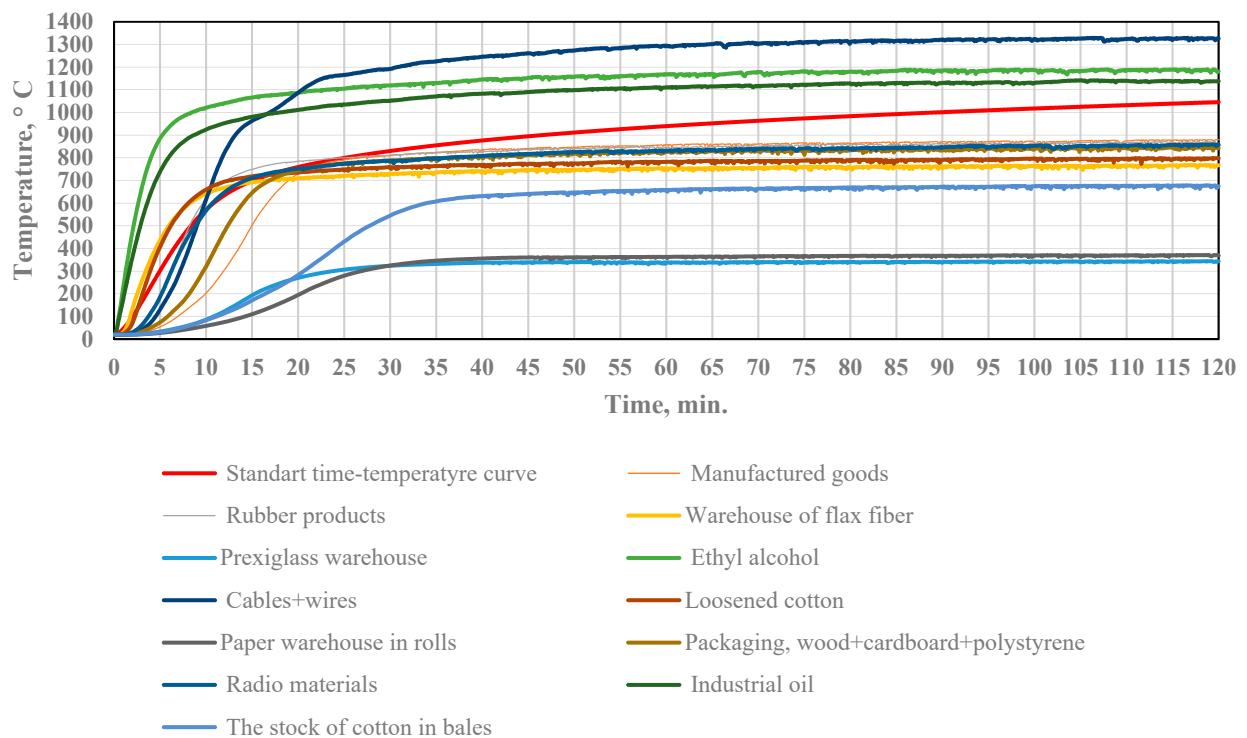


Figure 9. Rectangular 100 × 100 × 5 mm pipe.

For the considered fire loads, the heating time up to 400–700 °C for building structures can vary significantly and, in some cases, the time is lower than under the standard temperature conditions. Fire loads, such as flax fiber storage, ethyl alcohol, shredded cotton, industrial oil, and rubber goods provide values of the equivalent duration of fire that are higher than the duration of fire, which indicates an underestimation of the thermal

influence of actual fires on steel structures of warehouses under the effect of standard temperature conditions. Heating curves for various specimens under various temperature conditions are shown in Figures 7–9, and the equivalent fire duration depending on the type of fire load is shown in Figure 10.

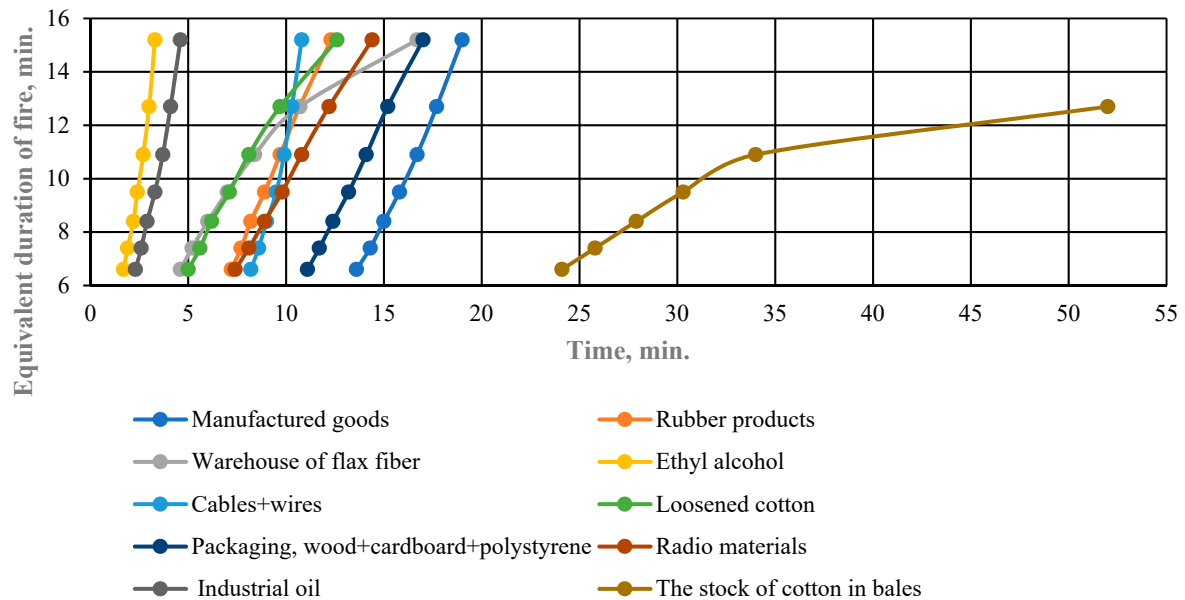


Figure 10. Equivalent fire duration depending on the type of fire load.

Figure 10 demonstrates that the equivalent fire duration for the following fire loads—flax fiber warehouse, ethanol, shredded cotton, industrial oil, and rubber technical goods—is bigger than fire duration, which means there was an underestimation of the heat influence of “real” fire on steel constructions for warehouse buildings for the standard temperature mode. The fire resistance loss by the bearing capacity for the roof truss at the most “critical real” temperature mode, obtained by modeling results, begins at the 2nd and 4th minutes for the “standard” temperature mode and at the 6th and 15th minutes for the critical temperatures of 400 and 700 °C, respectively. The numerical experiment results demonstrate that only the standard temperature mode application led to the underestimation of actual fire resistance limits for roof load-bearing constructions.

The methodology of the investigation can be used to analyze both the results obtained in the fired heater and under exposure to the radiant panel. Finally, the characteristics of the intumescent coatings exposed to different fire temperature conditions can be analyzed more properly in future research.

Further, comparing the flame-retardant properties of paint formed under fire conditions and “standard” temperature conditions, the authors introduce a new concept of “fire durability of flame-retardant paint”, which characterizes the ability of paint to retain its flame-retardant properties under fire conditions.

The FDS simulation results demonstrate that the temperature effect on the structure according to the standard temperature mode for the following fire loads—cables and wires, industrial oil, and ethanol—turned out to be less, which indicates an underestimation of the thermal effect on the structure. The results of modeling demonstrate that the heating time of the coating truss to 400–700 °C for the following fire loads—cables and wires, industrial oil, and ethyl alcohol—is less than the time obtained from the results of standard tests, which indicates an initial underestimation of the actual fire resistance of steel structures for warehouse buildings.

The results of the numerical experiment show that the heat flux density values can reach 280 kW/m², while in most cases, during the first 10 min, the heat flux density values did not exceed 50 kW/m².

The obtained heat flux density values were applied in a series of experiments to study the effect of heat flux on the formation of flame-retardant properties of paints under fire conditions.

3.3. Fire Test Results for Fire Paint

The results of heating for protected and unprotected constructions for various heat flows are presented in Figure 11.

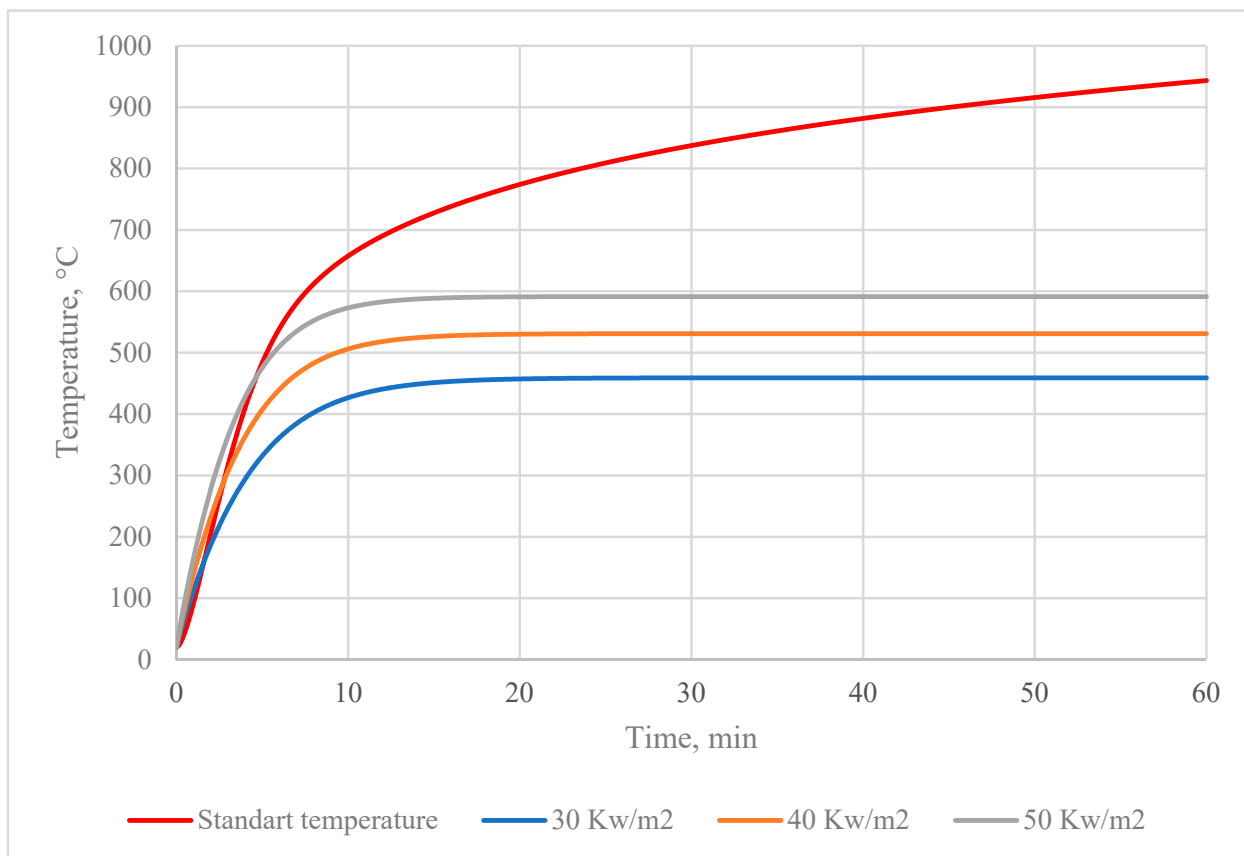


Figure 11. Temperature of unprotected specimens.

Figure 11 presents the temperature of the unprotected I-shaped steel column profile №20 for the standard temperature mode and the temperature of the unprotected steel plate (thickness 3 mm) for various heat flows.

Figure 12 presents the temperature of I-shaped steel column profile №20 with fire paint for the standard temperature mode.

Figure 13 presents the temperature of the steel plate (thickness 3 mm) with fire paint for various heat flows.

For the protected and unprotected specimens, the average temperature of steel was estimated as the average value for the thermocouple registrations. Therefore, within Equation (7), the effectiveness of the fire paint was calculated from point to point and is presented at Figure 14.

The experimental results demonstrate that fire paint effectiveness for the standard temperature mode is higher than for the heat flow of the radiative panel. It was also confirmed that fire paint effectiveness depends on the heat flow value; more precisely, the effectiveness was lower in the first 20 min at the density 30 Kw/m² compared with the densities 40 Kw/m² and 50 Kw/m², which varied unessentially.

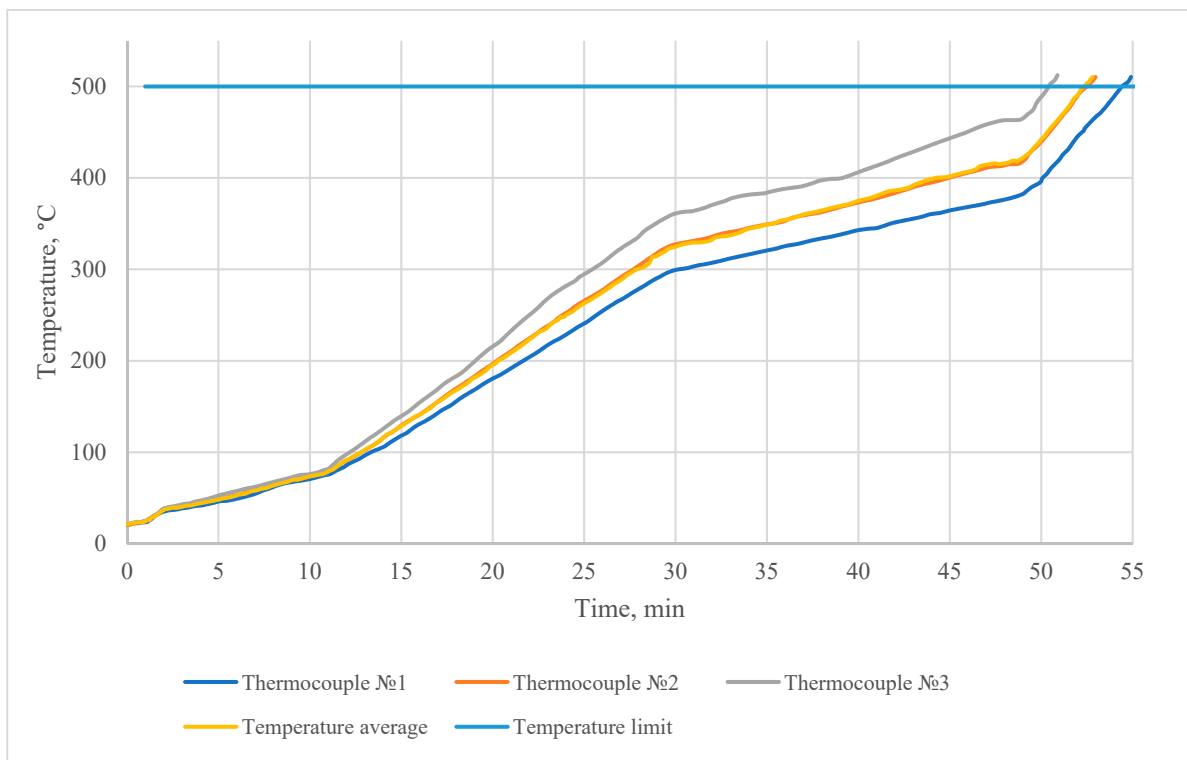


Figure 12. Temperature of steel specimen.

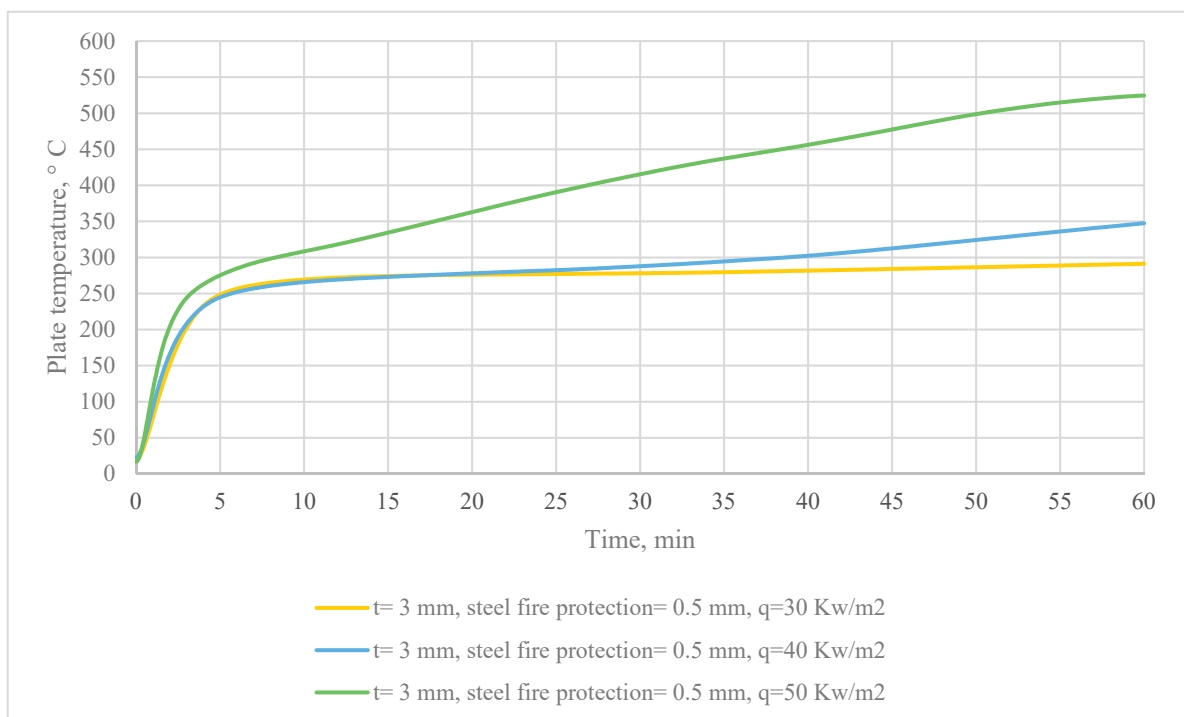


Figure 13. Curves of heating for steel plates (thickness 3 mm), with a heat flow density of 30 Kw/m², 40 Kw/m², and 50 Kw/m².

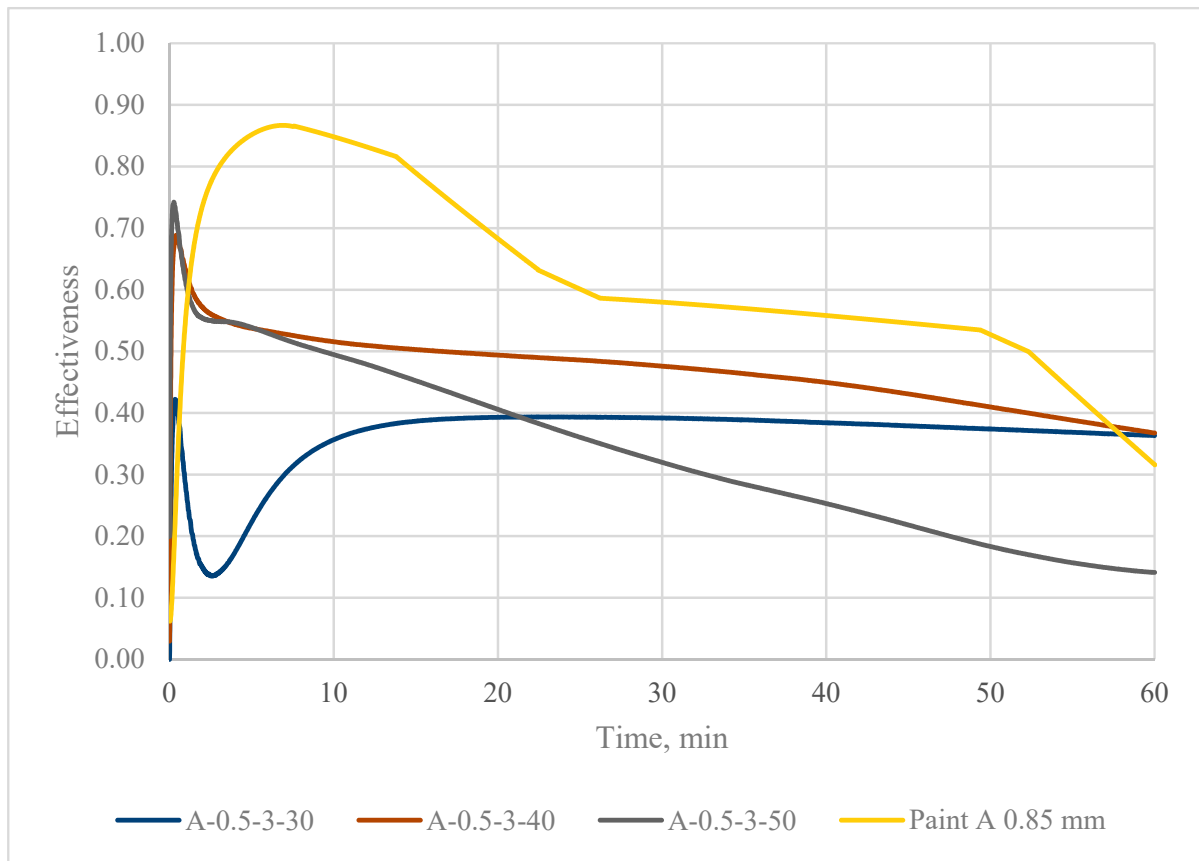


Figure 14. Fire paint effectiveness by experiment results.

4. Conclusions

Numerical experiments in the software package FDS confirmed that the temperature influence on load-bearing constructions for standard temperature mode was lower in three cases (total 12)—cable and wire, industrial oil, and ethanol—which demonstrated heat influence underestimation.

The results of heat modeling for constructions in the software package «ANSYS mechanical» confirmed that the heating time for the roof truss up to 400–700 °C for the mentioned fire loads was less than the time obtained by “standard” temperature mode heating, which demonstrated an underestimation of the actual fire resistance limits for steel constructions in the design projects of warehouse buildings.

The investigations of fire paint demonstrated that its effectiveness for various temperature modes varied and increased with the heat flow increasing. The application of the paint investigated for steel constructions to increase their fire resistance limits in the buildings, where the fire mode can essentially vary from “standard”, only based on standard fire test results, is incorrect because of the dependence of fire paint characteristics on “real” fire conditions.

The above-mentioned results demonstrate that the comparison of actual fire resistance limits and required normative values with the standard temperature mode, without considering the real fire load, can lead to an underestimation of the heat influence and actual fire resistance limit, which can have an adverse effect on the fire safety of warehouse buildings.

The evaluation of fire resistance limits for steel constructions with fire-retardant coatings at various fire conditions was based on a large number of experiments [43,44]. Taking into account the real fire loads led to the correct estimation of the actual fire resistance rating, which adversely affects the safety of the entire building. This is especially true for structures that can be used without fire protection.

Comparing the flame-retardant properties of paint formed under fire conditions and “standard” temperature conditions, the authors propose to introduce a new concept of “fire durability of flame-retardant paint”, which characterizes the ability of paint to retain its flame-retardant properties under fire conditions.

The assumption of underestimating the thermal effect of a standard temperature mode on steel structures of modern warehouse complexes was confirmed for 3 of the 12 considered fire loads, namely cables and wires, industrial oil, and ethyl alcohol.

Author Contributions: Conceptualization, T.E., D.K. and D.M.; methodology, T.E.; software, D.M.; validation, D.K.; formal analysis, D.K.; investigation, D.M.; resources, D.K.; data curation, T.E.; writing—original draft preparation, T.E. and D.K.; writing—review and editing, D.M.; visualization, D.M.; supervision, T.E. and D.K.; project administration, D.K.; funding acquisition, D.K. All authors have read and agreed to the published version of the manuscript.

Funding: This work was financially supported by the Ministry of Science and Higher Education of the Russian Federation (Project: theoretical and experimental design of new composite materials to ensure safety during the operation of buildings and structures under conditions of technogenic and biogenic threats #FSWG-2020-0007).

Institutional Review Board Statement: Not applicable.

Informed Consent Statement: Informed consent was obtained from all subjects involved in the study.

Data Availability Statement: The data presented in this study are available on request from the corresponding author.

Conflicts of Interest: All authors declare no conflict of interest concerning the representation or interpretation of reported research results.

References

- McKeen, L. *The Effect of Long Term Thermal Exposure on Plastics and Elastomers*, 2nd ed.; William Andrew: Norwich, NY, USA, 2021.
- Chen, Y.J.; Lai, Y.S.; Lin, Y.H. BIM-based augmented reality inspection and maintenance of fire safety equipment. *Autom. Constr.* **2020**, *110*, 103041. [[CrossRef](#)]
- Perera, D.; Upasiri, I.R.; Poologanathan, K.; Gatheeshgar, P.; Sherlock, P.; Hewavitharana, T.; Suntharalingam, T. Energy performance of fire rated LSF walls under UK climate conditions. *J. Build. Eng.* **2021**, *44*, 103293. [[CrossRef](#)]
- Johnston, R.P.D.; Lim, J.B.P.; Sonebi, M.; Wrzesien, A.M.; Armstrong, C. The Structural Behaviour in Fire of a Cold-Formed Steel Portal Frame Having Semi-Rigid Joints. Available online: <https://www.semanticscholar.org/paper/The-structural-behaviour-in-fire-of-a-cold-formed-Johnston-Lim/39855c2970a9929f79cf35afd48e0e5959808510> (accessed on 15 October 2021).
- Kruppa, I. Coolapse Temperature of Steel Structures. *J. Struct. Div.* **1979**, *105*, 1769–1788. [[CrossRef](#)]
- Dorn, I.E. *Progress in Understanding High Temperature Creep*; Grillet Memorial Lecture; ASTM: Philadelphia, PA, USA, 1962; p. 128.
- Tohr, I. Deformation and critical loads of steel beams under fire exposure conditions. *Stockholm* **1973**, *35*, 123.
- Yakovlev, A. *Calculation of Fire Resistance of Building Structures*; Stroiizdat: Moskow, Russia, 1988; p. 144.
- Molchadsky, I. *Fire in Enclosure*; Vniipo: Balashikha, Russia, 2005; p. 456.
- Roitman, V. *Engineering Solutions for Fire Resistance Evaluation for Designed and Reconstructed Buildings*; MGSU: Moskow, Russia, 2001; p. 382.
- Golovanov, V.; Kryuchkov, G. Steel Structures Fire Resistance Assessment under Standardized Fire Temperature Regimes. Fires and Incidents: Prevention. *Accid. Response* **2021**, *3*, 52–60.
- Guzman, N.H.C.; Kozine, I.; Lundteigen, M.A. An integrated safety and security analysis for cyber-physical harm scenarios. *Saf. Sci.* **2021**, *144*, 105458. [[CrossRef](#)]
- Wang, Q.; Zhang, C. Fire Safety Analysis of Building Partition Wall Engineering. *Procedia Eng.* **2018**, *211*, 747–754. [[CrossRef](#)]
- Nguyen, K.T.Q.; Navaratnam, S.; Mendis, P.; Zhang, K.; Barnett, J.; Wang, H. Fire safety of composites in prefabricated buildings: From fibre reinforced polymer to textile reinforced concrete. *Compos. Part B Eng.* **2020**, *187*, 107815. [[CrossRef](#)]
- Zhang, T.; Xi, J.; Qiu, S.; Zhang, B.; Luo, Z.; Xing, W.; Song, L.; Hu, Y. Facilely produced highly adhered, low thermal conductivity and non-combustible coatings for fire safety. *J. Colloid Interface Sci.* **2021**, *604*, 378–389. [[CrossRef](#)]
- Siddiqui, A.A.; Ewer, J.A.; Lawrence, P.J.; Galea, E.R.; Frost, I.R. Building Information Modelling for performance-based Fire Safety Engineering analysis—A strategy for data sharing. *J. Build. Eng.* **2021**, *42*, 102794. [[CrossRef](#)]
- Smith, T.D.; DeJoy, D.M.; Dyal, M.-A.; Pu, Y.; Dickinson, S. Multi-level safety climate associations with safety behaviors in the fire service. *J. Saf. Res.* **2019**, *69*, 53–60. [[CrossRef](#)] [[PubMed](#)]
- Sharma, A.; Singh, P.K.; Kumar, Y. An integrated fire detection system using IoT and image processing technique for smart cities. *Sustain. Cities Soc.* **2020**, *61*, 102332. [[CrossRef](#)]

19. Babkin, O.E.; Zybina, O.A.; Tanklevsky, J.I.T.; Mnatsakanov, S.S. Diagnostics of the application quality and efficiency of coke-forming fire-protective coatings for metal structures. *Ind. Coat.* **2014**, *7–8*, 50–54.
20. Zybina, O.A.; Babkin, O.E.; Tanklevsky, L.T.; Mnatsakanov, S.S. Formation of an intumescent layer during thermolysis of organophosphate-ammonium fire-retardant coatings. *World Electroplating*. **2014**, *5*, 56–58.
21. Leong, W.I.; Lo, O.L.I.; Cheng, F.T.; Cheong, W.M.; Seak, L.C.U. Using recombinant adhesive proteins as durable and green flame-retardant coatings. *Synth. Syst. Biotechnol.* **2021**, *6*, 369–376. [[CrossRef](#)] [[PubMed](#)]
22. Song, F.; Liu, T.; Fan, Q.; Li, D.; Ou, R.; Liu, Z.; Wang, Q. Sustainable, high-performance, flame-retardant waterborne wood coatings via phytic acid based green curing agent for melamine-urea-formaldehyde resin. *Prog. Org. Coat.* **2022**, *162*, 106597. [[CrossRef](#)]
23. Qi, L.; Qiu, S.; Xi, J.; Yu, B.; Hu, Y.; Xing, W. Construction of super-hydrophobic, highly effective flame retardant coating for cotton fabric with superior washability and abrasion resistance. *J. Colloid Interface Sci.* **2021**, *607*, 2019–2028. [[CrossRef](#)]
24. Rasoulipour, S.; Fleischmann, C.; Mercieca, L.; Adams, N. Flammability of engineered wood pyrolysis gases at anaerobic condition. *Fire Saf. J.* **2021**, *125*, 103424. [[CrossRef](#)]
25. Oswald, D. Homeowner vulnerability in residential buildings with flammable cladding. *Saf. Sci.* **2021**, *136*, 105185. [[CrossRef](#)]
26. Kalali, E.N.; Zhang, L.; Shabestari, M.E.; Croyal, J.; Wang, D.-Y. Flame-retardant wood polymer composites (WPCs) as potential fire safe bio-based materials for building products: Preparation, flammability and mechanical properties. *Fire Saf. J.* **2019**, *107*, 210–216. [[CrossRef](#)]
27. Li, P.; Liu, C.; Wang, B.; Tao, Y.; Xu, Y.-J.; Liu, Y.; Zhu, P. Eco-friendly coating based on an intumescent flame-retardant system for viscose fabrics with multi-function properties: Flame retardancy, smoke suppression, and antibacterial properties. *Prog. Org. Coat.* **2021**, *159*, 106400. [[CrossRef](#)]
28. Morandini, F.; Santoni, P.; Tramoni, J.; Mell, W. Experimental investigation of flammability and numerical study of combustion of shrub of rockrose under severe drought conditions. *Fire Saf. J.* **2019**, *108*, 102836. [[CrossRef](#)]
29. Dos Santos, D.M.; Goiato, M.C.; Moreno, A.; Pesqueira, A.; Dekon, S.F.D.C.; Guiotti, A.M. Effect of addition of pigments and opacifier on the hardness, absorption, solubility and surface degradation of facial silicone after artificial ageing. *Polym. Degrad. Stab.* **2012**, *97*, 1249–1253. [[CrossRef](#)]
30. Tong, C.; Zhang, S.; Zhong, T.; Fang, Z.; Liu, H. Highly fibrillated and intrinsically flame-retardant nanofibrillated cellulose for transparent mineral filler-free fire-protective coatings. *Chem. Eng. J.* **2021**, *419*, 129440. [[CrossRef](#)]
31. De Masi, R.F.; Ruggiero, S.; Vanoli, G.P. Acrylic white paint of industrial sector for cool roofing application: Experimental investigation of summer behavior and aging problem under Mediterranean climate. *Sol. Energy* **2018**, *169*, 468–487. [[CrossRef](#)]
32. Gatheeshgar, P.; Poologanathan, K.; Thamboo, J.; Roy, K.; Rossi, B.; Molken, T.; Perera, D.; Navaratnam, S. On the fire behaviour of modular floors designed with optimised cold-formed steel joist. *Structures* **2021**, *30*, 1071–1085. [[CrossRef](#)]
33. Roy, K.; Lim, J.B.; Lau, H.H.; Yong, P.M.; Clifton, G.C.; Johnston, R.P.; Wrzesien, A.; Mei, C.C. Collapse behaviour of a fire engineering designed single-storey cold-formed steel building in severe fires. *Thin-Walled Struct.* **2019**, *142*, 340–357. [[CrossRef](#)]
34. Johnston, R.P.D.; Lim, J.B.P.; Lau, H.H.; Xu, Y.; Sonebi, M.; Armstrong, C.G.; Mei, C.C. Finite-element investigation of cold-formed steel portal frames in fire. *Proc. Inst. Civ. Eng.-Struct. Build.* **2015**, *169*, 3–19. [[CrossRef](#)]
35. Johnston, R.; Lim, J.; Lau, H.H.; Xu, Y.; Sonebi, M.; Armstrong, C.; Switzer, C.; Mei, C. Cold-formed steel portal frames in fire: Full-scale testing and finite element analysis. *Struct. Eng.* **2014**, *92*, 44–50.
36. Shi, J.; Li, Y.; Chen, H. Application of Computer Integration Technology for Fire Safety Analysis. *Tsinghua Sci. Technol.* **2008**, *13*, 387–392. [[CrossRef](#)]
37. Kim, S.H.; Huh, K.Y. Assessment of The Finite-Volume Method and The Discrete Ordinate Method for Radiative Heat Transfer in a Three-Dimensional Rectangular Enclosure. *Numer. Heat Transf. Part B Fundam.* **1999**, *35*, 85–112.
38. Eremina, T.Y.; Fadeev, V.E.; Kadochnikova, E.N. Normative regulation of issues of ensuring fire safety of airport buildings. Prospects for the construction and development of airports in the Arctic region. In Proceedings of the Materials of the VI International Scientific and Practical Conference “Security Service in Russia: Experience, Problems, Prospects”, Saint Petersburg, Russia, 10 November 2014; pp. 80–83.
39. Chi, L.; Su, H.; Zio, E.; Zhang, J.; Li, X.; Zhang, L.; Fan, L.; Zhou, J.; Bai, H. Integrated Deterministic and Probabilistic Safety Analysis of Integrated Energy Systems with bi-directional conversion. *Energy* **2020**, *212*, 118685. [[CrossRef](#)]
40. Ushanov, V.V.; Fadeev, V.E.; Kharitonov, V.S.; Shchelkunov, V.I.; Pavlovsky, A.V.; Kosachev, A.A. Fire resistance and fire hazard of sandwich panels and proposals for amendments to regulatory legal acts on fire safety in terms of their application in buildings and structures for various functional purposes. *Fire Saf.* **2016**, *4*, 119–122.
41. Kumar, A.; Roy, K.; Uzzaman, A.; Lim, J.B.P. Finite element analysis of unfastened cold-formed steel channel sections with web holes under end-two-flange loading at elevated temperatures. *Adv. Steel Constr.* **2021**, *17*, 231–242.
42. Cui, M.; Li, J.; Chen, X.; Hong, W.; Chen, Y.; Xiang, J.; Yan, J.; Fan, H. A halogen-free, flame retardant, waterborne polyurethane coating based on the synergistic effect of phosphorus and silicon. *Prog. Org. Coat.* **2021**, *158*, 106359. [[CrossRef](#)]
43. Liu, C.; Zhang, T.; Luo, Y.; Wang, Y.; Li, J.; Ye, T.; Guo, R.; Song, P.; Zhou, J.; Wang, H. Multifunctional polyurethane sponge coatings with excellent flame retardant, antibacterial, compressible, and recyclable properties. *Compos. Part B Eng.* **2021**, *215*, 108785. [[CrossRef](#)]
44. Rahman, M.Z.; Kundu, C.K.; Nabipour, H.; Wang, X.; Song, L.; Hu, Y. Flame retardant and hydrophilic coatings on undyed and dyed polyamide 6.6 textiles: Clarifying the processing and performance. *Prog. Org. Coat.* **2021**, *163*, 106600. [[CrossRef](#)]